Synchronized spin-photon coupling in a microwave cavity

Vahram L. Grigoryan, Ka Shen, and Ke Xia*
The Center for Advanced Quantum Studies and Department of Physics, Beijing Normal University, Beijing 100875, China

(Received 10 February 2017; revised manuscript received 6 June 2018; published 6 July 2018)

We study spin-photon coupling in a cavity in the presence of a relative phase shift between two ferromagnetic resonance driving forces. We show that the anticrossing gap can be manipulated by varying the relative phase. Increasing the phase difference leads to narrowing the anticrossing gap between two hybridized modes and eventually phase-locked coupling when the relative phase equals π. The ferromagnetic resonance (FMR) and cavity modes become phase locked and oscillate at the same frequency near the resonance frequency. The characteristic FMR linewidth drop and transmission amplitude enhancement are demonstrated. The phase-resolved spin-photon coupling can be used both for phase imaging and for controlling coupling parameters.

DOI: 10.1103/PhysRevB.98.024406

I. INTRODUCTION

Strong interaction of light with matter in condensed-matter systems paves a way for exploring a wide range of different physical phenomena, for example, observation and manipulation of matter by light on an atomic scale as well as manipulation of the polariton [1] for quantum information technology. Recently, strong coupling between the light and the spin ensembles [2,3] has attracted great interest because of its experimental realization by locating magnetic materials with extremely low magnetic dissipation into high quality microwave cavities [4–12]. Coherent couplings between a single spin and the microwave cavity photons [13], magnons and a superconducting qubit [14], as well as cavity photons and magnons [9–12] have been reported. Indirect coupling between spins, mediated by a cavity, have also been achieved [15–17]. In addition to widely used microwave transmission measurements of magnon-photon coupling at room temperature, the electrical detection method has been recently demonstrated by Bai *et al.* [18]. Theoretically, the spin-photon coupling has been formulated by means of scattering theory [19] as well as the simple semiclassical model [18]. The relevance of the classical picture to the quantum-mechanical picture has been discussed elsewhere [20]. It was demonstrated that, although the coupling does not affect the intrinsic Gilbert damping, the FMR linewidth (ΔH) always increases [18] when the FMR frequency approaches the resonance.

To overcome the drawback of the FMR linewidth broadening due to coupling-induced extrinsic damping [18] in the strong-coupling regime we consider spin-photon coupling when, in addition to the magnetic component of the microwave field in the cavity, an additional local FMR driving force exists with a relative phase shift (Φ). In Fig. 1 we show the schematic of the system under study. In this setup the microwave signal from a broadband microwave generator G is directed via a coaxial cable to a rf power divider D [21,22], which coherently splits the microwave into two beams. One of them then travels through a microwave phase shifter [21,22] Φ in path A to an integrated [23] strip line on an insulator nonmagnetic layer. A ferromagnetic insulator lies on top of the strip line. The magnetic field, created by the microwave current in path A acts locally on the ferromagnetic insulator magnetization [24,25]. The other beam remains undisturbed and travels in path B through a coaxial cable to a microwave cavity resonator (the blue box in Fig. 1). Thus, the magnetization effectively feels two time-dependent magnetic fields, a local magnetic field $\mathbf{h}^{\mathrm{A}}$ and the magnetic component of the microwave inside the cavity $\mathbf{h}^{\mathrm{B}}$. We assume that the magnitude $h^{\mathrm{A}} = \delta h^{\mathrm{B}}$, where δ can be controlled by the divider. We show that for the coupling the relative phase (Φ) between the two fields plays an essential role in the FMR line shape. The spectrum of hybridized modes (polaritons) depends on the relative phase Φ. Particularly, the gap between two polariton modes can be tuned by Φ. More interestingly, the phase-locked coupling regime can be achieved by tuning the relative phase to π. As consequences of the phase-locked coupling, the FMR linewidth becomes very narrow, and the output microwave power is remarkably enhanced.

II. THEORETICAL FORMALISM

The simple semiclassical picture describing spin-phonon interaction in the cavity is based on the combination of a microwave LCR and Landau-Lifshitz-Gilbert (LLG) equations [18,26]. The coupling of the magnetization dynamics with a microwave is established via two classical coupling mechanisms. One is known as the Faraday induction [27] which induces a voltage in the LCR circuit due to the precessing magnetization. The other is governed by Ampere's law which supplies magnetic fields acting on the magnetization.

We consider the ferromagnetic insulator lying on the $\hat{\mathbf{x}}$-$\hat{\mathbf{z}}$ plane with an in-plane magnetic easy axis pointing in the $\hat{\mathbf{z}}$ direction due to crystal anisotropy, dipolar and external magnetic fields. The LCR circuit in the picture illustrates the theoretical model of the electromagnetic field in the cavity. The LCR circuit equation of two crossed coils parallel to the $\hat{\mathbf{x}}$ and $\hat{\mathbf{y}}$ directions in which the microwave current $\mathbf{j}^{\mathrm{B}}(t)$ is driven by

*Corresponding author: kexia@bnu.edu.cn

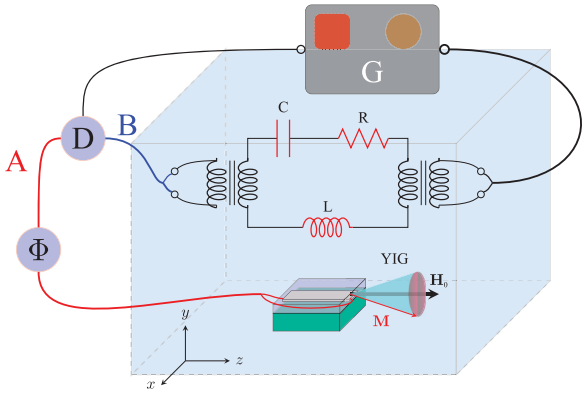

FIG. 1. Schematic of the system. The microwave signal is generated in "G". The generated signal is divided into "A" and "B" in rf power divider "D". The signal A travels through phase shifter "Φ" to a shorted strip line. The other signal travels directly to the cavity through path B. The microwave in the cavity is modeled by the LCR circuit, and YIG represents yttrium iron garnet, a typical magnetic insulator.

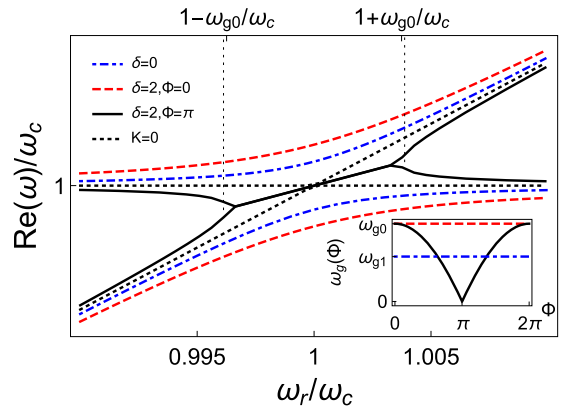

FIG. 2. The dispersion relation of polariton modes, i.e., the FMR mode coupled to the microwave mode for different values of δ and relative phase Φ. The inset shows the gap between two polariton modes ω_g as a function of the phase shift at $\omega_r = \omega_c$.

the rf voltage is

$$L\dot{\mathbf{j}}^{\mathrm{B}} + R\mathbf{j}^{\mathrm{B}} + (1/C)\int \mathbf{j}^{\mathrm{B}} dt = \mathbf{V}^{F}, \tag{1}$$

where L, C, and R are the inductor, the capacitor, and the resistor, respectively. The driving voltage $\mathbf{V}^{F}$ is induced by precessing magnetization according to Faraday induction,

$$V_x^F(t) = K_c L\dot{m}_y, \quad V_y^F(t) = -K_c L\dot{m}_x. \tag{2}$$

The magnetization precession in the magnetic sample is governed by the LLG equation [28],

$$\dot{\mathbf{m}} = -\mathbf{m}\times\gamma\mathbf{H} + \alpha\mathbf{m}\times\dot{\mathbf{m}}, \tag{3}$$

where $\mathbf{m} = \mathbf{M}/M_s$ is the magnetization direction in ferromagnetic insulator with M_s being the saturation magnetization. α is the intrinsic Gilbert damping parameter. $\mathbf{H} = \mathbf{H}_0 + \mathbf{h}^{\mathrm{A}} + \mathbf{h}^{\mathrm{B}}$ is the effective magnetic field with $\mathbf{H}_0 = H_0\hat{\mathbf{z}}$ being the sum of external magnetic, anisotropy, and dipolar fields aligned in the $\hat{\mathbf{z}}$ direction. $\mathbf{h}^{\mathrm{B}} = \mathbf{h}e^{-i\omega t}$ and $\mathbf{h}^{\mathrm{A}} = \delta\mathbf{h}^{\mathrm{B}}e^{-i\Phi}$ are the magnetic fields from paths B and A, respectively. Φ is the phase shift between them, and δ is the ratio between their amplitudes, which can be controlled in experiment [21,22]. Using the linearized form of the magnetization direction $\mathbf{m} \simeq \hat{\mathbf{z}} + \mathbf{m}_\perp e^{-i\omega t}$ the LLG equation becomes

$$m^+(\omega - \omega_r + i\alpha\omega) + (1 + \delta e^{i\Phi})\omega_m h^+ = 0, \tag{4}$$

where $m^+ = m_x + im_y$, $h^+ = h_x + ih_y$, $\omega_m = \gamma M_s$, and $\omega_r \simeq \gamma H_0$ with γ being the gyromagnetic ratio. The linearized equation of motion, i.e., Eq. (1) gives the other constraint and leads to

$$\Omega\begin{pmatrix} m^+ \\ h^+ \end{pmatrix} = 0,$$

with

$$\Omega \equiv \begin{pmatrix} \omega - \omega_r + i\alpha\omega & \omega_m(1+\delta e^{i\Phi}) \\ \omega^2 K^2 & \omega^2 + 2i\beta\omega\omega_c - \omega_c^2 \end{pmatrix}, \tag{5}$$

where Ampere's law,

$$h_x^{\mathrm{B}} = K_m j_y^{\mathrm{B}}, \quad h_y^{\mathrm{B}} = -K_m j_x^{\mathrm{B}} \tag{6}$$

has been applied. Here $j_{x,y}^{\mathrm{B}}$ represent the current components in the circuit. Parameters K_c and K_m are coupling parameters. $K \simeq \sqrt{K_c K_m}$, the cavity frequency is $\omega_c = 1/\sqrt{LC}$, and $\beta = R/(2L\omega_c)$ is the cavity mode damping. By solving Eq. (5) (det $\Omega = 0$) at a given magnetic field, we obtain the complex eigenfrequencies of ω. The two solutions of ω with positive real components correspond to the determine resonant frequencies, whereas their imaginary parts describe the damping of the corresponding modes.

III. RESULTS AND DISCUSSION

In Fig. 2 we plot the dispersion spectrum Re[$\omega(\omega_r)$] (normalized by ω_c) for different values of phase-shift Φ. The dotted lines correspond to the cavity mode and Kittel's mode in the absence of spin-photon coupling. We set equal damping for FMR and LCR as $\alpha = \beta = 0.002$, $\omega_m = 0.075\omega_c$, and the coupling parameter is $K = 0.01$ [29] with $\omega_c/2\pi = 10.5$ GHz.

We now discuss the behaviors resulting from the different values of the free parameters δ and Φ. First, the blue dashed-dotted lines in Fig. 2 are the spectra (normalized by ω_c) in the case when no second path exists. This corresponds to the usual spin-photon coupling with the characteristic anticrossing of two modes [18]. Here, the gap between two modes at FMR resonance ($\omega_r = \omega_c$) is proportional to the coupling constant K and in the strong-coupling regime ($K > \alpha,\beta$) can be approximated to be $\omega_{g1} \equiv \omega_g(\delta = 0) = K\sqrt{2\omega_m\omega_c}$ [29]. Besides this widely studied regime, we adopt two sets of parameters: (i) $\Phi = 0$, $\delta = 2$ and (ii) $\Phi = \pi$, $\delta = 2$.

In Fig. 2 the red dashed curve shows the spectrum in case (i), and the solid black curve is for case (ii). In the case where no phase shift is introduced, i.e., case (i), the coupling increases. Moreover, as shown in the inset of Fig. 2, tuning the relative phase (with fixed δ) changes the size of the gap in the range of the coupling bandwidth [the range of FMR frequencies, projected by the two vertical dotted lines with $\omega_{g0} \equiv \omega_g(\delta = 2, \Phi = 0) = K\sqrt{6\omega_m\omega_c}$ where the polariton

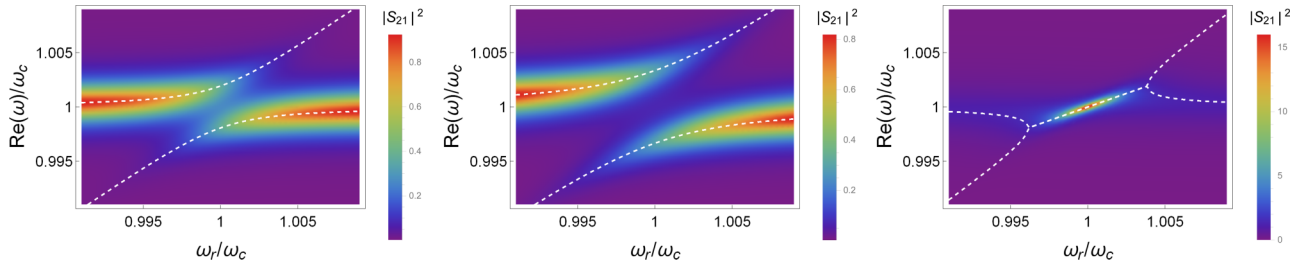

FIG. 3. The dashed lines stand for the dispersion relation of the coupled modes. The colored area shows the transmission amplitude defined in Eq. (7) for (a) $\delta = 0$, (b) $\delta = 2$, $\Phi = 0$, and (c) $\delta = 2$, $\Phi = \pi$.

modes occur]. The relative phase shift causes different features in the spin-photon coupling spectrum. In the spectrum, for $\Phi = 0$ the frequency of the FMR mode decreases with increasing frequency of the cavity mode at $\omega_r < \omega_c$ and increases at $\omega_r > \omega_c$. Such a behavior reverses at $\Phi = \pi$: Due to the phase shift, the FMR mode frequency increases at $\omega_r < \omega_c$ and decreases at $\omega_r > \omega_c$. As a consequence, a gap is opened due to the coupling in the $\Phi = 0$ case, and for $0 \leqslant \Phi \leqslant \pi$ it decreases with increasing Φ. The frequencies of the two modes get "pulled" [30] toward each other (see the inset of Fig. 2) and eventually lead to synchronization at $\Phi = \pi$ where the two modes start to share the same frequency $(\omega_c + \omega_r)/2$. Note that, although the studies of synchronization usually refer to the nonlinear system [30,31], the synchronization has also been demonstrated in the purely linear systems [32–36]. Our study here thus provides a different version of synchronization in linear system. The dependence of the gap on Φ at $\omega_r = \omega_c$ can be approximately expressed by $\omega_g(\Phi) = \omega_{g0}|\cos(\Phi/2)|$.

The physical picture of phase-locked coupling in the present system is the following: A localized magnetic moment "feels" the effective magnetic field from two microwave sources and changes its direction which generates a voltage in the LCR circuit due to the Faraday induction. This voltage causes a current in the circuit, which, in turn, produces a magnetic field due to Ampere's law and exerts a torque on the magnetization. When there is no phase shift between $\mathbf{h}^{\mathrm{A}}$ and $\mathbf{h}^{\mathrm{B}}$ ($\Phi = 0$), energy exchange takes place between microwaves in the cavity and oscillating magnetization where one drives the other. In the case of two driving forces with opposite phases ($\Phi = \pi$), the energy loss due to damping of the magnetization precession is compensated by the torque coming from $\mathbf{h}^{\mathrm{A}}$. As a result, instead of performing as a dissipation channel in the usual case [18], the ferromagnetic insulator under $\Phi = \pi$ absorbs energy from the $\mathbf{h}^{\mathrm{A}}$ field and behaves as a pumping source of the $\mathbf{h}^{\mathrm{B}}$ field, leading to an enhancement of the $\mathbf{h}^{\mathrm{B}}$ field.

To study the signal power enhancement, we calculate the transmission amplitude using input-output formalism from Eq. (5) [18,24,37],

$$\Omega\begin{pmatrix} m^+ \\ h^+ \end{pmatrix} = \begin{pmatrix} 0 \\ \omega^2 h_0^+ \end{pmatrix},$$

and

$$S_{21} = \Gamma h^+/h_0^+ = \Gamma \frac{\omega^2(\omega + i\alpha\omega - \omega_r)}{\det\,\Omega}, \qquad (7)$$

where h_0^+ is the input magnetic field driving the system and $\Gamma = 2\beta$ characterizes the cavity/cable impedance mismatch [18]. In Fig. 3 we plot the spectrum of the coupled system where the dashed line is $\mathrm{Re}[\omega(\omega_r)]$ and the colored area represents the transmission amplitude. In Fig. 3(a) we show the transmission amplitude when $\delta = 0$ where the usual anticrossing features in the strong-coupling regime are observed. Figure 3(b) shows the results with increased coupling ($\delta = 2$) but without phase shift ($\Phi = 0$). The phase-locking case is shown in Fig. 3(c) where the transmission amplitude—proportional to transmission power—is lower at FMR frequencies far from resonance and increases dramatically when ω_r approaches ω_c. Figure 4 shows the transmission amplitude evolution as a function of ω at different fixed values of FMR frequency ω_r. At FMR frequencies outside the synchronization regime, i.e., $|\omega_r - \omega_c| \gg \omega_{g0}$, the transmission amplitude is almost not affected by the FMR, and the transmission is determined solely by the cavity mode and is equal to that of the empty cavity. Tuning the FMR frequency towards the resonance of the cavity mode $|\omega_r - \omega_c| \lesssim \omega_{g0}$, the transmission amplitude increases and reaches its maximum (black solid curve in Fig. 4) at resonance $\omega_r = \omega_c$.

To analyze the second characteristic feature of the phase-locked coupling, namely, the FMR linewidth drop, we solve Eq. (5) to obtain ω_r as a function of ω. In contrast to the solution for ω, here we have only one solution. The real part of $\omega_r(\omega)$ gives the FMR spectrum whereas the imaginary part gives the linewidth $\Delta H = \mathrm{Im}[\omega_r(\omega)]/\mathrm{Re}[\omega_r(\omega)]$. It has been demonstrated, that in the coupled cavity FMR system, the FMR linewidth is modified by the coupling [18]. In Fig. 5 we plot the normalized FMR linewidth as a function of ω. The dotted curve shows that in the absence of spin-photon coupling the linewidth is constant and determined by the damping constant α. In the

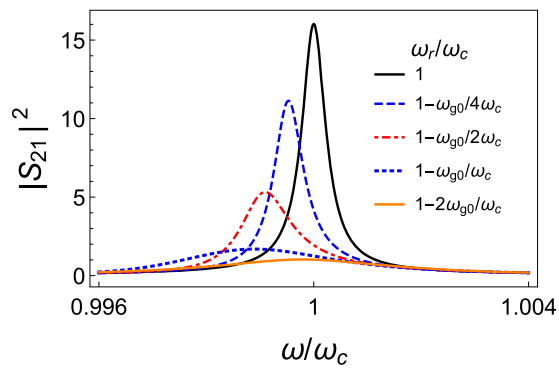

FIG. 4. The transmission amplitude in the phase-locked regime as a function of ω at different values of the FMR frequency.

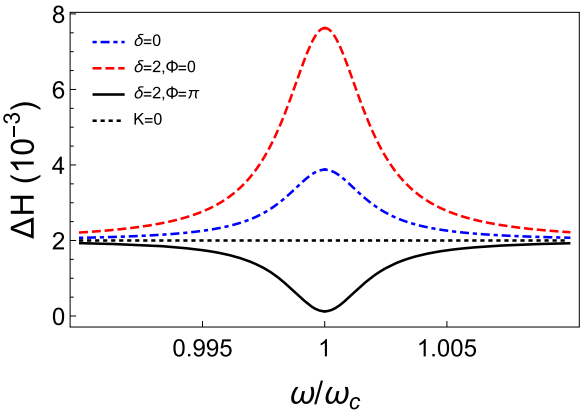

FIG. 5. Normalized FMR linewidth ΔH as a function of ω.

presence of spin-photon coupling but in the absence of beam A ($\delta = 0$) the normalized linewidth is broadened by the coupling around the resonance (blue dot-dashed line in Fig. 5) [18], and the broadening is even larger for (i) ($\Phi = 0$, $\delta = 2$), shown by the red dashed curve. In the case when a relative phase-shift $\Phi = \pi$ is introduced, the linewidth decreases (black solid curve in Fig. 5) near the resonance frequency as expected for the phase-locked coupling.

In contrast to $\delta = 0$ discussed in Ref. [18] where the FMR linewidth always increases as the FMR approaches the resonant coupling condition, no matter whether $\alpha < \beta$ or $\alpha > \beta$, here both transmission coefficient and FMR linewidth depend on the interplay between dampings of the two oscillators and coupling strength. At the resonance ($\omega = \omega_c$), the FMR linewidth can be expressed as

$$\Delta H = \frac{2\alpha\beta + K^2(\omega_m/\omega_c)[\delta\,\cos(\Phi) + 1]}{2\beta - \delta K^2(\omega_m/\omega_c)\sin(\Phi)}, \tag{8}$$

which reduces to

$$\Delta H = \alpha + (1-\delta)\frac{K^2(\omega_m/\omega_c)}{2\beta}, \tag{9}$$

at $\Phi = \pi$. It turns out that for $\delta < 1$ the FMR linewidth increases in the presence of spin-photon coupling due to the coupling-induced damping enhancement [18]. However, for $\delta > 1$, the second driving force exerts an antidamping torque, which compensates the intrinsic damping and coupling-induced FMR linewidth broadening. For a very small damping and strong coupling, instability is reached when the phase-shifted driving force is very strong and the effective linewidth becomes negative. In this case, the magnetization dynamics may become very complicated and possibly leads to magnetization reversal. A systematic study of complicated dynamic phases in this regime would be useful but beyond the scope of the linearized equations used in this paper. One can find the condition of stability in such a way that the FMR linewidth is positive, that is, the phase-shifted driving force cannot exceed the critical strength to fully compensate the intrinsic and coupling-induced dampings. This condition leads to (for $\delta = 2$) $\alpha\beta = K^2\omega_m/2\omega_c$. Thus, large cavity damping can be compensated by low Gilbert damping. Although the calculations here are performed with equal damping parameters, the synchronization behavior is the same for other damping parameters satisfying the $\Delta H > 0$ condition, where ΔH is defined in Eq. (8) at resonant FMR frequency.

IV. SUMMARY

To summarize, we study the spin-photon coupling in a cavity in the presence of two FMR driving forces with a relative phase shift between them. We show that the anticrossing gap between the two cavity-FMR hybridized modes can be controlled by the phase shift. Increasing the phase shift leads to a reduction of the gap and the phase-locked spectrum when the relative phase equals π. In this regime the two modes start to oscillate at the same frequency in the $|\omega_r - \omega_c| \lesssim \omega_{g,0}$ range. The FMR linewidth drop and power enhancement are demonstrated.

A technical challenge for the experimental realization of the proposed synchronized coupling is to isolate the local field $\mathbf{h}^{\mathrm{A}}$ from the cavity so that it will not introduce any unexpected influence on the cavity. This might be possible if the magnetic insulator film is capped by microwave absorbing and metallic shielding layers [38]. We note that in the proposed setup the cavity quality could be severely reduced when it is loaded by a strip line. However, the change in cavity damping due to the reduced quality factor is not essential, and the predicted phenomenon will survive as long as $\Delta H > 0$ is satisfied. Another option is to use an open cavity [9] where one path travels through a phase shifter to a waveguide attached to a ferromagnetic insulator film [39], whereas the other goes to a horn antenna, exposed to the magnetic insulator. In that case the effect of the magnetic field from the horn antenna on the waveguide mode can be shielded by the covering part (enclosing the waveguide overlapping area on the opposite side of the magnetic insulator).

ACKNOWLEDGMENTS

We thank M. Weides and I. Boventer for discussions about the experimental setup. This work was financially supported by the National Key Research and Development Program of China (Grant No. 2017YFA0303300) and the National Natural Science Foundation of China (Grants No. 61774017, No. 11734004, and No. 21421003). K.S. acknowledges the Recruitment Program of Global Youth Experts and the support by the Fundamental Research Funds for the Central Universities (Grant No. 2018EYT02).

[1] D. L. Mills and E. Burstein, Rep. Prog. Phys. **37**, 817 (1974).
[2] R. H. Dicke, Phys. Rev. **93**, 99 (1954).
[3] M. Tavis and F. W. Cummings, Phys. Rev. **170**, 379 (1968).
[4] Y. Kubo, F. R. Ong, P. Bertet, D. Vion, V. Jacques, D. Zheng, A. Dréau, J. F. Roch, A. Auffeves, F. Jelezko, J. Wrachtrup, M. F. Barthe, P. Bergonzo, and D. Esteve, Phys. Rev. Lett. **105**, 140502 (2010).

[5] R. Amsuss, C. Koller, T. Nobauer, S. Putz, S. Rotter, K. Sandner, S. Schneider, M. Schrambock, G. Steinhauser, H. Ritsch, J. Schmiedmayer, and J. Majer, Phys. Rev. Lett. **107**, 060502 (2011).

[6] D. I. Schuster, A. P. Sears, E. Ginossar, L. DiCarlo, L. Frunzio, J. J. L. Morton, H. Wu, G. A. D. Briggs, B. B. Buckley, D. D. Awschalom, and R. J. Schoelkopf, Phys. Rev. Lett. **105**, 140501 (2010).

[7] S. Probst, H. Rotzinger, S. Wunsch, P. Jung, M. Jerger, M. Siegel, A. V. Ustinov, and P. A. Bushev, Phys. Rev. Lett. **110**, 157001 (2013).

[8] K. Sandner, H. Ritsch, R. Amsuss, C. Koller, T. Nobauer, S. Putz, J. Schmiedmayer, and J. Majer, Phys. Rev. A **85**, 053806 (2012).

[9] H. Huebl, C. W. Zollitsch, J. Lotze, F. Hocke, M. Greifenstein, A. Marx, R. Gross, and S. T. B. Goennenwein, Phys. Rev. Lett. **111**, 127003 (2013).

[10] Y. Tabuchi, S. Ishino, T. Ishikawa, R. Yamazaki, K. Usami, and Y. Nakamura, Phys. Rev. Lett. **113**, 083603 (2014).

[11] X. Zhang, C.-L. Zou, L. Jiang, and H. X. Tang, Phys. Rev. Lett. **113**, 156401 (2014).

[12] N. J. Lambert, J. A. Haigh, S. Langenfeld, A. C. Doherty, and A. J. Ferguson, Phys. Rev. A **93**, 021803(R) (2016).

[13] J. J. Viennot, M. C. Dartiailh, A. Cottet, and T. Kontos, Science **349**, 408 (2015).

[14] Y. Tabuchi, S. Ishino, A. Noguchi, T. Ishikawa, R. Yamazaki, K. Usami, and Y. Nakamura, Science **349**, 405 (2015).

[15] S. Haroche and J.-M. Raimond, *Exploring the Quantum: Atoms, Cavities and Photons* (Oxford University Press, Oxford, 2006).

[16] A. Blais, R.-S. Huang, A. Wallraff, S. M. Girvin, and R. J. Schoelkopf, Phys. Rev. A **69**, 062320 (2004).

[17] A. Wallraff, D. I. Schuster, A. Blais, L. Frunzio, J. Majer, S. Kumar, S. M. Girvin, and R. J. Schoelkopf, Nature (London) **431**, 162 (2004).

[18] L. Bai, M. Harder, Y. P. Chen, X. Fan, J. Q. Xiao, and C.-M. Hu, Phys. Rev. Lett. **114**, 227201 (2015).

[19] Y. Cao, P. Yan, H. Huebl, S. T. B. Goennenwein, and G. E. W. Bauer, Phys. Rev. B **91**, 094423 (2015).

[20] M. Harder, L. H. Bai, C. Match, J. Sirker, and C. M. Hu, Sci. China: Phys., Mech. Astron. **59**, 117511 (2016).

[21] A. Wirthmann, X. Fan, Y. S. Gui, K. Martens, G. Williams, J. Dietrich, G. E. Bridges, and C.-M. Hu, Phys. Rev. Lett. **105**, 017202 (2010).

[22] Z. X. Cao, W. Lu, L. Fu, Y. S. Gui, and C.-M. Hu, Appl. Phys. A **111**, 329 (2013).

[23] J. C. Lau, R. P. Malmgren, and K. Lui, Integrated waveguide/stripline transition, U.S. Patent No. 5,311,153 (17 July 1994).

[24] M. Harder, Z. X. Cao, Y. S. Gui, X. L. Fan, and C.-M. Hu, Phys. Rev. B **84**, 054423 (2011).

[25] Y. Gui, L. Bai, and C.-M. Hu, Sci. China: Phys., Mech. Astron. **56**, 124 (2013).

[26] N. Bloembergen and R. V. Pound, Phys. Rev. **95**, 8 (1954).

[27] T. J. Silva, C. S. Lee, T. M. Crawford, and C. T. Rogers, J. Appl. Phys. **85**, 7849 (1999).

[28] T. L. Gilbert, IEEE Trans. Magn. **40**, 3443 (2004).

[29] L. Bai, K. Blanchette, M. Harder, Y. P. Chen, X. Fan, J. Q. Xiao, and C.-M. Hu, IEEE Trans. Magn. **52**, 1000107 (2016).

[30] A. Slavin and V. Tiberkevich, IEEE Trans. Magn. **45**, 1877 (2009).

[31] W. H. Rippard, M. R. Pufall, S. Kaka, T. J. Silva, S. E. Russek, and J. A. Katine, Phys. Rev. Lett. **95**, 067203 (2005).

[32] B. Heinrich, Y. Tserkovnyak, G. Woltersdorf, A. Brataas, R. Urban, and G. E. W. Bauer, Phys. Rev. Lett. **90**, 187601 (2003).

[33] Y. Tserkovnyak, A. Brataas, G. E. W. Bauer, and B. I. Halperin, Rev. Mod. Phys. **77**, 1375 (2005).

[34] D. Zhang, X.-Q. Luo, Y.-P. Wang, T.-F. Li, and J. Q. You, Nat. Commun. **8**, 1368 (2017).

[35] N. R. Bernier L. D. Toth, A. K. Feofanov, and T. J. Kippenberg, arXiv:1709.02220.

[36] M. Harder, L. Bai, P. Hyde, and C.-M. Hu, Phys. Rev. B **95**, 214411 (2017).

[37] M. Harder, P. Hyde, L. Bai, Ch. Match, and C.-M. Hu, Phys. Rev. B **94**, 054403 (2016).

[38] F. Qin and C. Brosseau, J. Appl. Phys. **111**, 061301 (2012).

[39] X. F. Zhu, M. Harder, A. Wirthmann, B. Zhang, W. Lu, Y. S. Gui, and C.-M. Hu, Phys. Rev. B **83**, 104407 (2011).